Chapter 8 Weight Estimation

8.1. Introduction

Statistical weight equations, although capable of producing landing gear group weights quickly and generally accurately, do not respond to all the variations in landing gear design parameters. In addition, the equations are largely dependent on the database of existing aircraft. For future large aircraft, such weight data is virtually non-existent. Thus, it is desirable that an analytical weight estimation method which is more sensitive than statistical methods to variations in the design of the landing gear should be adopted. The objectives are to allow for parametric studies involving key design considerations that drive landing gear weight, and to establish crucial weight gradients to be used in the optimization process.

Based on the procedures described in this chapter, algorithms were developed to size and estimate the weight of the structural members of the landing gear. The weight of non-structural members were estimated using statistical weight equations. The two were then combined to arrive at the final group weight.

8.2. Current Capabilities

The primary shortcoming of statistical methods is that only a limited number of weight-affecting parameters are considered, *e.g.*, length of the strut, material ultimate strength, vertical load, and number of tires. As a result, it is extremely difficult to distinguish landing gears with different geometric arrangements using these parameters alone. Statistical weight equations are also constrained by what has been designed in the past, *i.e.*, if an unconventional design or a new class of aircraft such as the proposed ultra-high-capacity transport is involved, there might not be sufficient data to develop a statistical base for the type of landing gear required.

The majority of existing equations calculate the landing gear weight purely as a function of aircraft takeoff gross weight. It is the simplest method for use in sizing analysis, and is adopted in ACSYNT as well as by Torenbeek [5] and General Dynamics, as given by Roskam [3]. The Douglas equation used in the blended-spanload concept [41] also falls into this category. Other weight equations, *e.g.*, Raymer [42] and FLOPS (Flight Optimization System) [13], include the length of the landing gear in the calculation and

thus are able to produce estimates which reflect the effect of varying design parameters to some extent.

Actual and estimated landing gear weight fractions are presented in Fig. 8.1. Figure 8.1a provides comparisions for estimates which only use MTOW. Figure 8.1b provides comparisions with methods which take into account more details, specifically the gear length. As shown in Fig. 8.1a, for an MTOW up to around 200,000 lb, the estimated values from ACSYNT and Torenbeek are nearly equal. However, as the MTOW increases, completely different trends are observed for the two equations: an increasing and then a decreasing landing gear weight fraction is predicted by ACSYNT, whereas a continual increasing weight fraction is predicted by Torenbeek. As for the Douglas equation, an increasing weight fraction is observed throughout the entire MTOW range. Upon closer examination of the data presented, it was found that only a small number of actual landing gear weight cases are available to establish trends for aircraft takeoff weight above 500,000 pounds. In addition, even within the range where significant previous experience is available, the data scatter between actual and estimated values is too large to draw conclusions on the accuracy of existing weight equations. Evidently a systematic procedure is needed to validate the reliability of the statistical equations, and provide another level of estimation.

8.3. Analytical Structural Weight Estimation

Analytical weight estimation methods are capable of handling varying configurations and geometry, in addition to design parameters used in the statistical methods. As typified by Kraus [43] and Wille [44], the procedure consists of five basic steps: definition of gear geometry, calculation of applied loads, resolution of the loads into each structural member, sizing of required member cross-sectional areas, and calculation of component and total structural weight. Although these studies provided an excellent guideline toward the development of an MDO-compatible analysis algorithm, detailed discussions in the area of load calculations and structural design criteria were not included in the papers. To fill the gap, simplified loading conditions were determined from Torenbeek and the FAA [20], and structural analyses were developed as part of this work. Loading conditions are presented in Section 8.3.2., and the structural analyses are presented in Sections 8.3.3. and 8.3.4. and Appendix B.

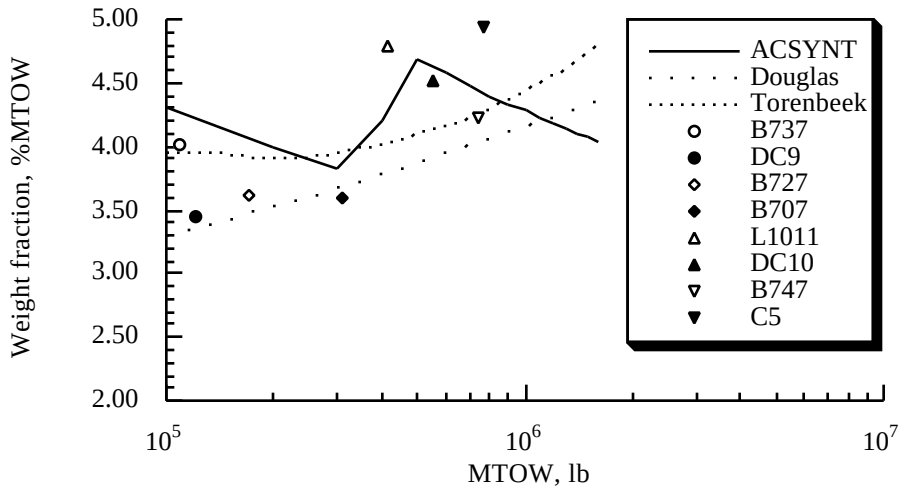

a) Pure weight fraction equations

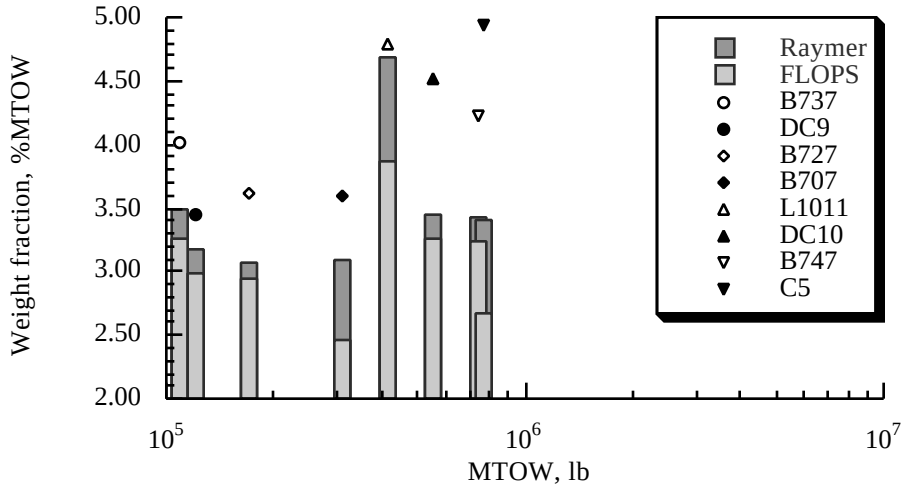

b) Weight fraction equations with landing gear length

Figure 8.1 Landing gear weights comparison

8.3.1 Generic Landing Gear Model

A generic model consisting of axles, truck beam, piston, cylinder, drag and side struts, and trunnion is developed based on existing transport-type landing gears. Since most, if not all, of the above items can be found in both the nose and main gear, the model can easily be modified to accommodate both types of assembly without difficulty. Although the torsion links are presented for completeness, they are ignored in the analysis since their contributions to the final weight are minor.

The model shown in Fig. 8.2 represents a dual-twin-tandem configuration. The model can be modified to represent a triple-dual-tandem or a dual-twin configuration with relative ease, *i.e.*, by including a center axle on the truck beam, or replacing the bogie with a single axle, respectively. The model assumes that all structural components are of circular tube construction except in the case of the drag and side struts, where an I-section can be used depending on the configuration. When used as a model for the nose gear, an additional side strut arranged symmetrically about the plane of symmetry is included.

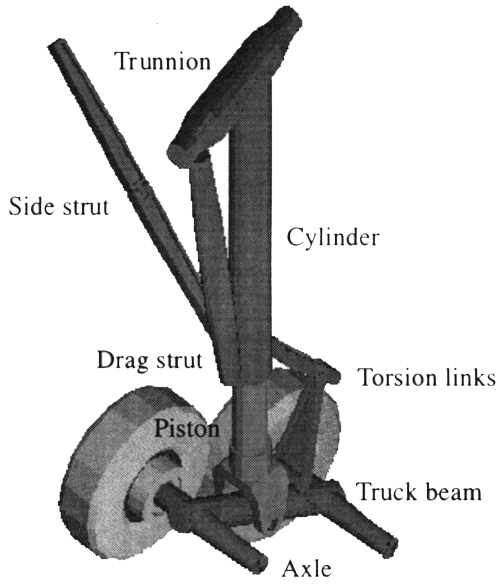

Figure 8.2 Generic landing gear model

For added flexibility in terms of modeling different structural arrangements, the landing gear geometry is represented by three-dimensional position vectors relative to the aircraft reference frame. Throughout the analysis, the *xz*-plane is chosen as the plane of symmetry with the *x*-axis directed aft and the *z*-axis upward. The locations of structural components are established by means of known length and/or point locations, and each point-to-point component is then defined as a space vector in the *x, y,* and *z* directions. Based on this approach, a mathematical representation of the landing gear model is created and is shown in Fig. 8.3.

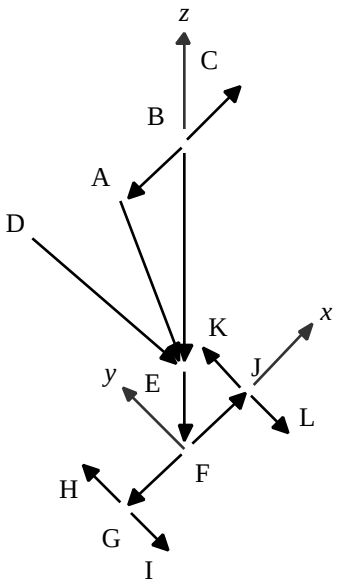

Vector	Description
BA	Forward trunnion
BC	Aft trunnion
BE	Cylinder
AE	Drag strut
DE	Side strut
EF	Piston
FG, FJ	Truck beam
GH, GI, JK, JL	Axles

Figure 8.3 Mathematical representation of the landing gear model

8.3.2. Applied Loads

External loads applied to the gear assemblies can be divided into dynamic and static loads: the former occurs under landing conditions while the latter occurs during ground operations. As listed in Table 8.1, seven basic loading conditions have been selected for analysis with the applied loads calculated as specified in FAR Part 25 [20]. These conditions are also illustrated in Fig. 8.4.

Table 8.1 Basic landing gear loading conditions [20]

Dynamic	Static
Three-point level landing	Turning
One-wheel landing	Pivoting
Tail-down landing	
Lateral drift landing	
Braked roll	

The corresponding aircraft attitudes are shown in Fig. 8.4, where symbols D, S and V are the drag, side and vertical forces, respectively, n is the aircraft load factor, W is aircraft maximum takeoff or landing weight, T is the forward component of inertia force, and I is the inertial moment in pitch and roll conditions necessary for equilibrium. The subscripts m and n denote the main and nose gear, respectively.

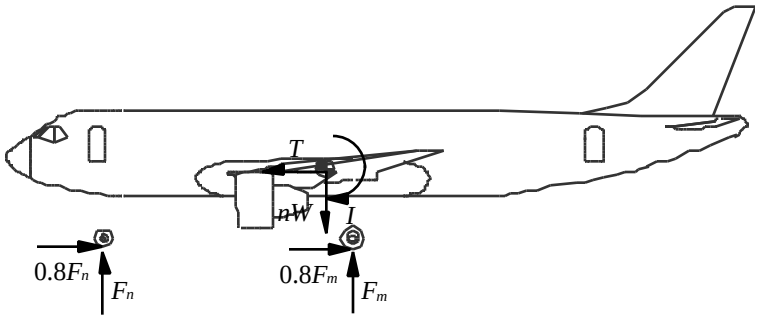

a) Three-point level landing

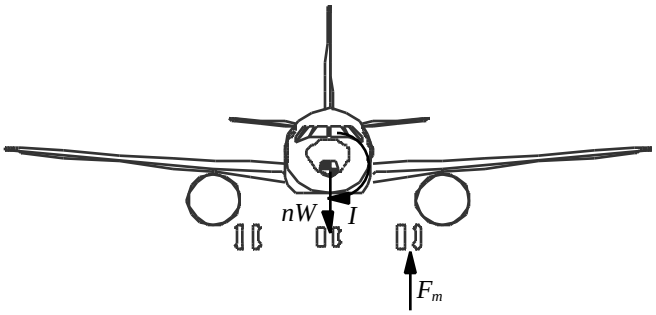

b) One-wheel landing

Figure 8.4 Aircraft attitudes under dynamic and static loading conditions [20]

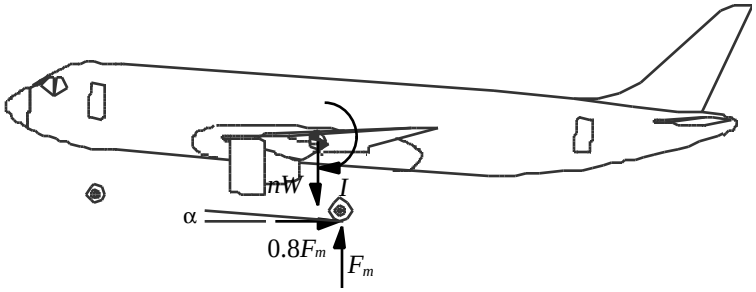

c) Tail-down landing

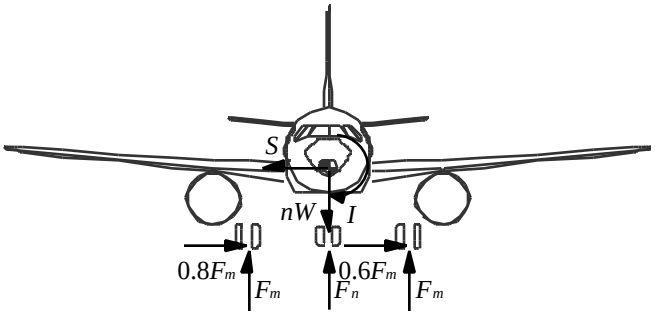

d) Lateral drift landing

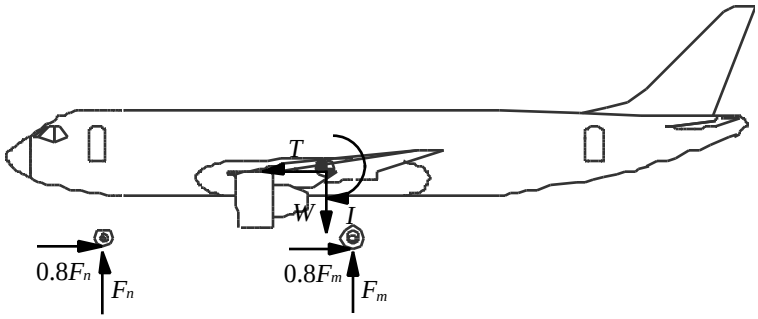

e) Braked roll

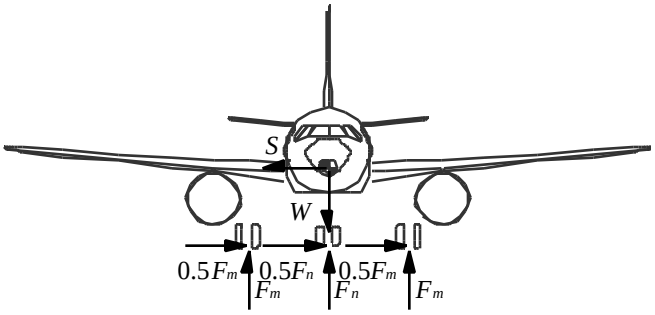

f) Turning

Figure 8.4 Aircraft attitudes under dynamic and static loading conditions [20] (continued)

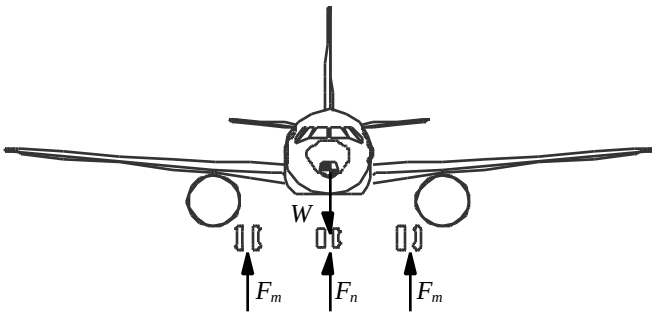

g) Pivoting

Figure 8.4 Aircraft attitudes under dynamic and static loading conditions [20] (concluded)

For the dynamic landing conditions listed in Table 8.1, the total vertical ground reaction (F) at the main assembly is obtained from the expression [43]

$$F = \frac{cW}{\eta S \cos\alpha}\left(\frac{V_s^2}{g} + S\cos\alpha\right) \tag{8.1}$$

where c is the aircraft weight distribution factor, η is the gear efficiency factor, S is the total stroke length, α is the angle of attack at touchdown, V_s is the sink speed, and g is the gravitational acceleration. Although the vertical force generated in the gear is a direct function of the internal mechanics of the oleo, in the absence of more detailed information Eq. (8.1) provides a sufficiently accurate approximation.

The maximum vertical ground reaction at the nose gear, which occurs during low-speed constant deceleration, is calculated using the expression [5, p. 359]

$$F_n = \frac{l_m + a_x / g \quad h_{cg}}{l_m + l_n} W \tag{8.2}$$

For a description of variables and the corresponding values involved in Eq. (8.2), refer to Chapter Four, Section Two.

The ground loads are initially applied to the axle-wheel centerline intersection except for the side force. As illustrated in Fig. 8.5, the side force is placed at the tire-ground contact point and replaced by a statically equivalent lateral force in the y direction and a couple whose magnitude is the side force times the tire rolling radius.

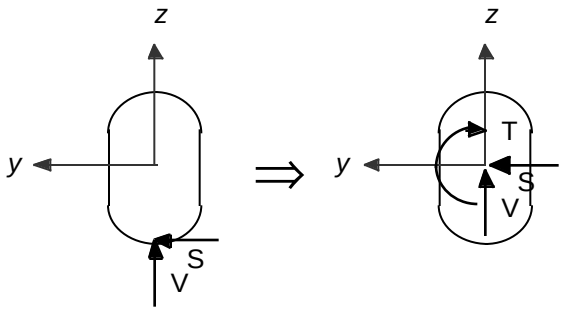

Figure 8.5 Location of the applied ground loads

To determine the forces and moments at the selected structural nodes listed in Table 8.2, the resisting force vector ($\mathbf{F}_{res}$) is set equal and opposite to the applied force vector ($\mathbf{F}_{app}$)

$$\mathbf{F}_{res} = -\mathbf{F}_{app} \tag{8.3}$$

whereas the resisting moment vector ($\mathbf{M}_{res}$) is set equal and opposite to the sum of the applied moment vector ($\mathbf{M}_{app}$) and the cross product of the space vector ($\mathbf{r}$) with $\mathbf{F}_{app}$

$$\mathbf{M}_{res} = -\left(\mathbf{M}_{app} + \mathbf{r} \times \mathbf{F}_{app}\right) \tag{8.4}$$

Table 8.2 Selected structural nodes description

Node	Description	Location (Figure 8.3)
1	Axle-beam centerline intersection	G/J
2	Beam-piston centerline intersection	F
3	Drag/side/shock strut connection	E
4	Cylinder-trunnion centerline intersection	B

8.3.3. Forces and Moment Resolution

Three-dimensional equilibrium equations are used to calculate member end reactions. Internal forces and moments are then determined from equilibrium by taking various cross-sectional cuts normal to the longitudinal axis of the member. To ensure that the information is presented in a concise manner, the methods used in the analysis are discussed only in general terms, while detailed derivations are compiled and presented in Appendix B.

8.3.3.1. Coordinate Transformation

Given that the mathematical landing gear model and the external loads are represented in the aircraft reference frame, transformation of nodal force and moment vectors from the aircraft to body reference frames are required prior to the determination of member internal reactions and stresses. The body reference frames are defined such that the x_3-axis is aligned with the component's axial centerline, and *xz*-plane is a plane of symmetry if there is one. The transformation is accomplished by multiplying the force and moment vectors represented in the aircraft reference frame by the transformation matrix $\mathbf{L}_{BA}$ [45, p. 117]

$$\mathbf{F}_B = \mathbf{L}_{BA}\mathbf{F}_A \tag{8.5}$$

$$\mathbf{M}_B = \mathbf{L}_{BA}\mathbf{M}_A \tag{8.6}$$

where subscripts *A* and *B* denote the aircraft and landing gear body reference frames, respectively. By inspection of the angles in Fig. 8.7, where subscripts 1, 2, and 3 denote the rotation sequence from the aircraft (*x*, *y*, and *z*) to the body (x_3, y_3, and z_3) reference frame, the three localized transformation matrices are [45, p. 117]

$$\mathbf{L}_1(\varphi_1) = \begin{bmatrix} 1 & 0 & 0 \\ 0 & \cos\varphi_1 & \sin\varphi_1 \\ 0 & -\sin\varphi_1 & \cos\varphi_1 \end{bmatrix} \tag{8.7a}$$

$$\mathbf{L}_2(\varphi_2) = \begin{bmatrix} \cos\varphi_2 & 0 & -\sin\varphi_2 \\ 0 & 1 & 0 \\ \sin\varphi_2 & 0 & \cos\varphi_2 \end{bmatrix} \tag{8.7b}$$

$$\mathbf{L}_3(\varphi_3) = \begin{bmatrix} \cos\varphi_3 & \sin\varphi_3 & 0 \\ -\sin\varphi_3 & \cos\varphi_3 & 0 \\ 0 & 0 & 1 \end{bmatrix} \tag{8.7c}$$

Thus, the matrix $\mathbf{L}_{BA}$ is given as [45, p. 117]

$$\mathbf{L}_{BA} = \mathbf{L}_3(\varphi_3)\mathbf{L}_2(\varphi_2)\mathbf{L}_1(\varphi_1) \tag{8.8}$$

or

$$\mathbf{L}_{BA} = \begin{bmatrix} \cos\varphi_2 \cos\varphi_3 & \sin\varphi_1 \sin\varphi_2 \cos\varphi_3 + \cos\varphi_1 \sin\varphi_3 & -\cos\varphi_1 \sin\varphi_2 \cos\varphi_3 + \sin\varphi_1 \sin\varphi_3 \\ -\cos\varphi_2 \sin\varphi_3 & -\sin\varphi_1 \sin\varphi_2 \sin\varphi_3 + \cos\varphi_1 \cos\varphi_3 & \cos\varphi_1 \sin\varphi_2 \sin\varphi_3 + \sin\varphi_1 \cos\varphi_3 \\ \sin\varphi_2 & -\sin\varphi_1 \cos\varphi_2 & \cos\varphi_1 \cos\varphi_2 \end{bmatrix} \quad (8.9)$$

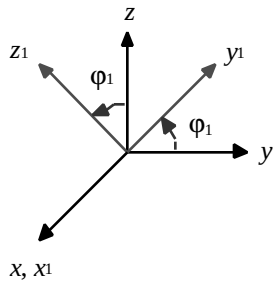

a) About the x, x_1-axis

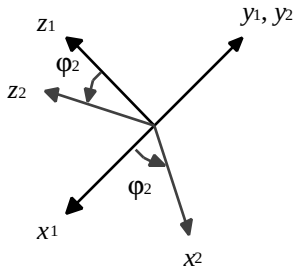

b) About the y_1, y_2-axis

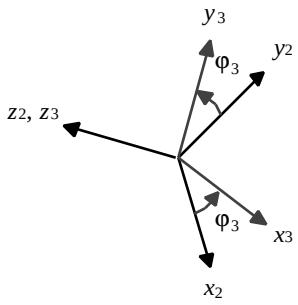

c) About the z_2, z_3-axis

Figure 8.6 Orientation of the axes and the corresponding rotation angles

8.3.3.2. The Main Assembly

The main assembly drag strut and side strut structure is modeled as a space truss consisting of ball-and-socket joints and two-force members. As shown in Fig. 8.7 the loads applied to the cylinder consist of the side strut forces (F_{side}), drag strut force (F_{drag}), an applied force with components F_x, F_y, and F_z, and an applied couple with moment components C_x, C_y, and C_z. Internal axial actions are obtained using the method of sections. Equilibrium equations are then used to determine the magnitude of the internal axial forces in the isolated portion of the truss.

The shock strut cylinder, in addition to supporting the vertical load, also resists a moment due to asymmetric ground loads about the z-axis. This moment is transmitted from the truck beam assembly to the cylinder though the torsion links. Note that in the tandem configurations, the moment about the y-axis at the piston-beam centerline is ignored because of the pin-connection between the two. However, this moment must be considered in the dual-twin configuration, where the moment is resisted by the integrated axle/piston structure.

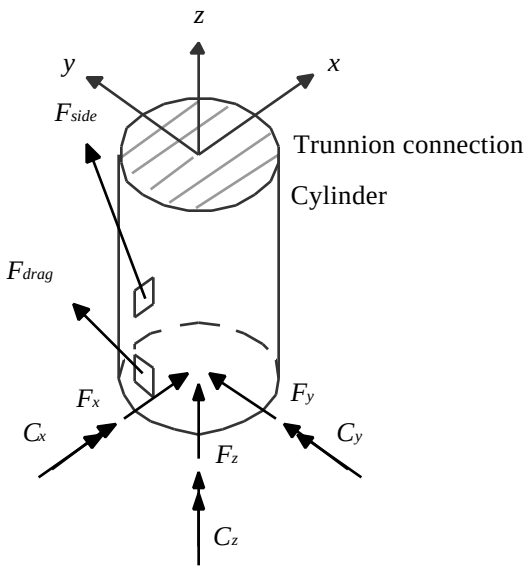

Figure 8.7 Idealized main assembly cylinder/drag/side struts arrangement

8.3.3.3. The Nose Assembly

As mentioned in the geometric definition section, an additional side strut, arranged symmetrically about the *xz*-plane, is modeled for the nose assembly. The addition of the second side strut results in a structure that is statically indeterminate to the first degree as shown in Fig. 8.8. The reactions at the supports of the truss, and consequently the internal reactions, can be determined by Castigliano's theorem [46, p. 611]

$$u_j = \frac{\partial U}{\partial P_j} = \sum_{i=1}^{n} \frac{F_i l_i}{A_i E} \frac{\partial F_i}{\partial P_j} \tag{8.10}$$

where u_j is the deflection at the point of application of the load P_j, E is the modulus of elasticity, and l, F, and A are the length, internal force, and cross-sectional area of each member, respectively. The theorem gives the generalized displacement corresponding to the redundant, P_j, which is set equal to a value compatible with the support condition. This permits the solution of the redundant, and consequently all remaining internal actions, via equilibrium. As detailed in Appendix B, Section Two, the procedure is to first designate one of the reactions as redundant, and then determine a statically admissible set of internal actions in terms of the applied loads and the redundant load. By assuming a rigid support which allows no deflection, Eq. (8.10) is set to zero and solved for P_j.

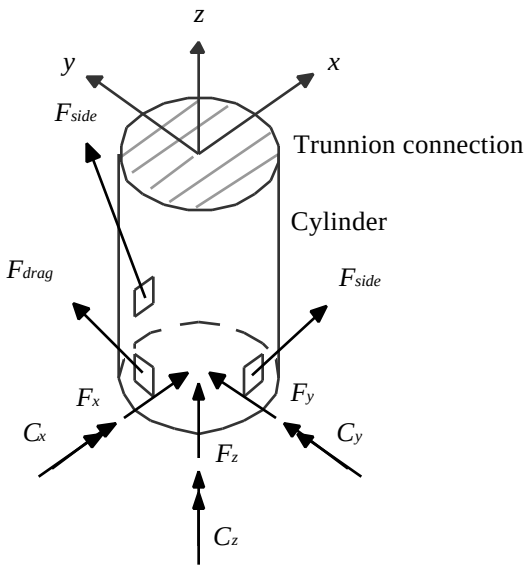

Figure 8.8 Idealized nose gear cylinder/drag/side struts arrangement

8.3.3.4. The Trunnion

When the gear is in the down-and-locked position, the trunnion is modeled as a prismatic bar of length L with clamped ends. As shown in Fig. 8.9, the trunnion is subjected to a force with components F_x, F_y, and F_z, and a couple with components C_y and C_z, at axial position $x = l_1$, where $0 < l_1 < L$ and $0 \le x \le L$. Clamped end-conditions at $x = 0$ and $x = L$ yield ten homogeneous conditions, five at each end. At the load point $x = l_1$, there are five continuity conditions, *i.e.*, u, v, w, v', and w', and five jump conditions corresponding to point-wise equilibrium of the internal actions and the external loads.

The linear elastic response of the trunnion is statically indeterminate, but can be readily solved by the superposition of an extension problem for the x-direction displacement component $u(x)$, a bending problem in the xy-plane for the y-direction displacement $v(x)$, and a bending problem in the xz-plane for the z-direction displacement $w(x)$. Using classical bar theory, the governing ordinary differential equation (ODE) for $u(x)$ is second order, while the governing ODEs for $v(x)$ and $w(x)$ are each fourth order. The governing equations are solved in the open intervals $0 < x < l_1$ and $l_1 < x < L$, where the 20 constants of integration (c_i) resulting from integration of the ODEs with respect to x are determined using the boundary and transition conditions as given above. Details of the solution are given in Appendix B, Section Three.

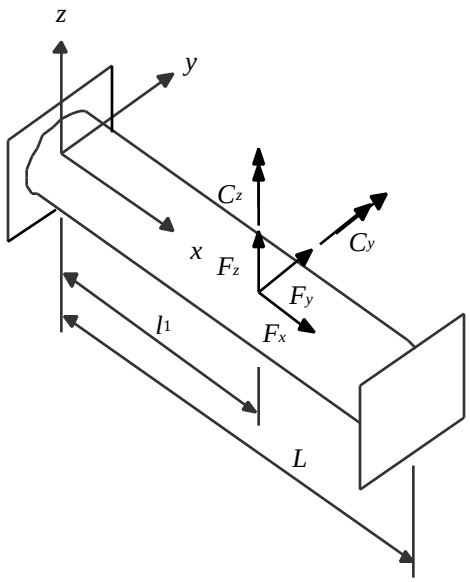

Figure 8.9 Trunnion modeled as a clamped-clamped bar

8.3.4. Member Cross-sectional Area Sizing

With the resolution of various ground loads, each structural member is subjected to a number of sets of internal actions that are due to combinations of extension, general bending, and torsion of the member. To ensure that the landing gear will not fail under the design condition, each structural member is sized such that the maximum stresses at limit loads will not exceed the allowables of the material and that no permanent deformation is permitted.

A description of selected cuts near major component joints and supports is given in Table 8.3. Normal and shear stresses acting on the cross section due to the internal actions were calculated at these locations and used in the sizing of the required member cross-sectional area.

Table 8.3 Sections description

Section	Description	Location (Figure 8.3)
1	Axle-beam centerline intersection	G/J
2	Beam-piston centerline intersection	F
3	Piston	E
4	Cylinder/struts connection	E
5	Cylinder/trunnion centerline intersection	B
6	Forward trunnion mounting	A
7	Aft trunnion mounting	C
8	Drag strut	A
9	Side strut	D

8.3.4.1. Normal and Shear Stresses In a Thin-walled Tube

The normal stresses induced on the structural members are determined by combining the effects of axial load and combined bending, while the shear stresses are determined by combining the effects of torsion and shear forces due to bending [47].

The normal stress (t_{xx}) due to combined axial force and bending moments is given as

$$\tau_{xx} = \frac{N}{A} + \frac{M_y}{I_{yy}} z - \frac{M_z}{I_{zz}} y \tag{8.11}$$

where N is the maximum axial force, A is the cross-sectional area of the member, M_y and M_z are the internal moment components, and I_{yy} and I_{zz} are the second area moments about the y- and z-axis, respectively. As shown in Appendix B, Section Four, the extremum values of the normal stress on a circular-tube cross section under combined axial and bending actions are

$$\tau_{xx_{\substack{max\\or\\min}}} = \frac{N}{A} \pm \frac{1}{\pi r^2 t}\sqrt{M_y^2 + M_z^2} \tag{8.12}$$

where r is the mean radius of the tube and t is the wall thickness. In the case of drag and side struts, the last two terms in Eq. (8.11) are zero since both members are modeled as pin-ended two-force members, thus,

$$\tau_{xx} = \frac{N}{A} \tag{8.13}$$

The shear stress(τ_{xs}) due to combined transverse shear forces and torque is given as

$$\tau_{xs} = \frac{q(s)}{t} + (\tau_{xs})_{torque} \tag{8.14}$$

where q is the shear flow due to bending of a thin-walled tube, see Fig. 8.10. Given that

$$tan\theta_{max} = -\frac{V_z}{V_y} \tag{8.15}$$

where θ_{max} is the polar angle where the bending shear flow attains an extremum value and V_y and V_z are the shear forces components, Eq. (8.14) then becomes

$$\tau_{xs_{\substack{max\\or\\min}}} = \frac{1}{\pi r t}\left(\frac{T}{2r} \pm \sqrt{V_y^2 + V_z^2}\right) \tag{8.16}$$

where T is the applied torque. Details of the solution are given in Appendix B, Section Four.

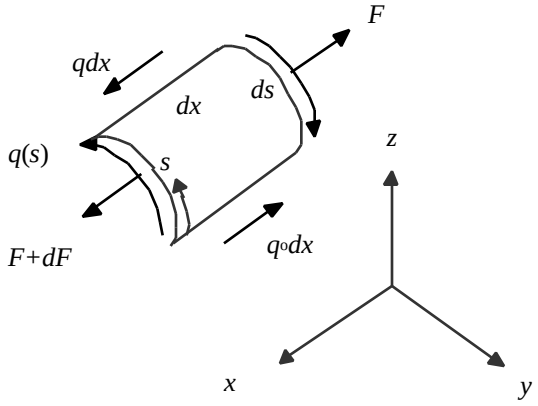

Figure 8.10 Shear flow around a tube

8.3.4.2. Design Criteria

Although aircraft structural design calls for multiple load paths to be provided to give fail-safe capability, the concept cannot be applied in the design of the landing gear structures. Accordingly, the gear must be designed such that the fatigue life of the gear parts can be safely predicted or that the growth of cracks is slow enough to permit detection at normal inspection intervals [4].

Von Mises yield criterion for ductile materials combined with a factor of safety is used to determine the stress limit state. The Mises equivalent stress is given as [46, p. 368]

$$\sigma_{Mises} = \sqrt{\tau_{xx}^2 + 3\tau_{xs}^2} \tag{8.17}$$

and the factor of safety is defined as the ratio of the yield stress of the material to the Mises equivalent stress, that is,

$$F.S. = \frac{\sigma_{yield}}{\sigma_{Mises}} \tag{8.18}$$

If this value is less than the specified factor of safety, the cross-sectional area of the component is increased until the desired value is attained.

In addition to material limit state, the critical loads for column buckling of the drag and side struts are considered because of the large slenderness ratio associated with these members. The slenderness ratio is defined as the length of the member (L) divided by the minimum radius of gyration (ρ_{min}). Assuming a perfectly aligned axial load, the critical buckling load for a pin-ended two-force member can be calculated using Euler's formula [46, p. 635]

$$N_{cr} = \frac{\pi^2 EI}{L^2} \tag{8.19}$$

where E is the modulus of elasticity. In the case of a member with circular cross section, the moment of inertia I of the cross section is the same about any centroidal axis, and the member is as likely to buckle in one plane as another. For other shapes of the cross section, the critical load is computed by replacing I in Eq. (8.19) with I_{min}, the minimum second moment of the cross section (bending about the weak axis). Note that the Euler's formula only accounts for buckling in the long column mode and is valid for large slenderness ratio, *e.g.*, $L/\rho_{min} > 80$ for 6061-T6 Aluminum alloy. For slenderness ratio below this range, intermediate column buckling should be considered [48].

8.3.4.3. Sizing of the Cross-sectional Area

For thin-walled circular tubes, the cross-sectional area of the member is given as

$$A = \pi D t \tag{8.20}$$

where the mean diameter (D) and design thickness (t) are both design variables. Instead of using these two variables in the analysis directly, the machinability factor (k), which is defined as the mean diameter divided by the wall thickness, is introduced to account for tooling constraints [49]. The factor is defined as

$$k = \frac{D}{t} \tag{8.21}$$

and has an upper limit of 40. For the thin-wall approximation to be valid in the structural analysis k > 20. Thus, the machinability factor is limited to

$$20 \leq k \leq 40 \tag{8.22}$$

By replacing t in Eq. (8.20) with Eq. (8.21) and using D as a limiting design variable, the desired cross-sectional area can then be determined by iterating on k. Note that the lower limit of k given in Eq. (8.21) may be violated in some instances. For structural members such as the axles, the truck beam, and piston, which typically feature k values in the mid-teens, St. Venant's theory for torsion and flexure of thick-walled bars [50] should be used to calculate shear stresses. Essentially, the problem is broken down into torsion and bending problems and the shear stresses are calculated separately based on the linear theory of elasticity.

In general, the diameter of each cylindrical component is a function of either the piston or wheel dimension. In the case of shock strut, it is assumed that the internal pressure is evenly distributed across the entire cross-sectional area of the piston. That is, the piston area is a function of the internal oleo pressure (P_2) and the maximum axial force, that is,

$$A = \frac{N}{P_2} = \frac{\pi D_p^2}{4} \tag{8.23}$$

where D_p is the outer diameter of the piston. Rearrangement of Eq. (8.23) gives

$$D_p = \sqrt{\frac{4N}{\pi P_2}} \tag{8.24}$$

Assuming a perfect fit between the piston lining and the inner cylinder wall, the minimum allowable mean diameter of the cylinder is obtained by adding the wall thickness of the cylinder to the piston outer diameter. To reduce the level of complexity, the minimum allowable mean diameter of the trunnion is assumed to be identical to that of the cylinder. Similar assumptions are made concerning the axle and truck beam, except that the outer diameter of the above members is treated as a function of the diameter of the wheel hub. In the case of the axle, the maximum allowable mean diameter is obtained by subtracting the axle wall thickness from the hub diameter.

For the thin-walled I-section bar shown in Fig. 8.11, the cross-sectional area and principal centroidal second area moments are

$$A = t(2b + h) \tag{8.25}$$

$$I_{yy} = t\left[\frac{h^3}{12} + 2b\left(\frac{h}{2}\right)^2\right] \tag{8.26}$$

and

$$I_{zz} = \frac{b^3 t}{6} \tag{8.27}$$

where h is the web height and b is the width of the two flanges. Assume that $I_{yy} > I_{zz}$, algebraic manipulations then result in

$$\frac{h}{b} > \sqrt{2} \tag{8.28}$$

and the z-axis is the weak axis in bending. The cross-sectional area is related to the second area moment by the minimum radius of gyration, that is,

$$A = \frac{I_{zz}}{\rho_{min}^2} \tag{8.29}$$

or for the I-section

$$\rho_{min} = \frac{b}{\sqrt{12 + 6h/b}} \tag{8.30}$$

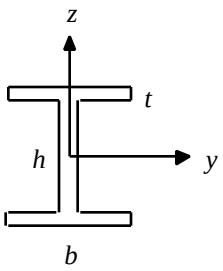

Figure 8.5 I-section truss bar

Since only the cross-sectional area is used in the weight computation, it is not necessary to determine the actual dimensions of the sectional height and width. Instead, one of the dimensions, usually the height, is treated as a function of the piston diameter and the other is then calculated with a predetermined *h*/*b* ratio.

8.3.5. Structural Weight Calculation

The final step of the analytical procedure is to calculate the weight of each member based on its cross-sectional area, length, and the material density. Recall that seven different loading conditions were examined in the analysis, which results in seven sets of cross-sectional areas for each member. To ensure that the component will not fail under any of the seven loading conditions, the maximum cross-sectional area from the sets is selected as the final design value. Component weights are then calculated by multiplying each of the cross-sectional areas by the corresponding length and material density. The summation of these calculations then becomes the structural weight of the idealized analytical model.

8.3.6. Validation of the Analysis

For analysis validation purposes, the landing gears for the Boeing Models 707, 727, 737 and 747 were modeled and analyzed. The estimated structural weight, which includes the axle/truck, piston, cylinder, drag and side struts, and trunnion, accounts for roughly 75 percent of the total structural weight that can be represented in the model [43]. The remaining 25 percent of the gear structural weight is made up of the torsion links, fittings, miscellaneous hardware, and the internal oleo mechanism, *e.g.*, the metering tube, seals, oil, pins, and bearings. Note that actual and estimated structural weights presented in Tables 8.4 and 8.5 only account for the components that were modeled in the analysis.

Table 8.4 Main assembly structural weight comparison

Aircraft	Estimated, lb	Actual, lb	Est/Act
B737	784	768	1.02
B727	1396	1656	0.84
B707	2322	2538	0.91
B747	9788	11323	0.86

Table 8.5 Nose assembly structural weight comparison

Aircraft	Estimated, lb	Actual, lb	Est/Act
B737	107	145	0.74
B727	171	327	0.52
B707	159	222	0.72
B747	1010	1439	0.70

Differences between the actual and estimated structural weights can be attributed to several factors. First, the models analyzed are extremely simple, *i.e.*, structural members were represented with simple geometric shapes and no considerations have been given to fillet radii, local structural reinforcement, bearing surfaces, *etc.* As for the analysis itself, simplistic equations were used to calculate the applied static and dynamic loads, and idealized structural arrangements were used to determine the member internal reactions. However, it should be noted that the results are consistent with Kraus' original analysis; where an average of 13 percent deviation was cited [43].

8.4. Landing Gear Group Weight Estimation

Although proven to be far more responsive to variations in design parameters, it is unlikely that an analytical tool will replace statistical methods. In fact, both methods should be used as complements to one another. This is particularly true in the calculation of the landing gear group weight, where the analytical and statistical methods can be used to determine the structural and non-structural component weights, respectively.

For large transports, landing gear structural weight accounts for roughly 57 percent of the landing gear group weight. The remaining weight is made up by the rolling stock and controls; the former accounts for roughly 34 percent of the total weight, while the latter accounts for the last nine percent. Note that the weights of the tires, wheels and brakes that make up the rolling stock have already been determined in previous chapters and no additional calculations are required. As for the controls, *i.e.*, actuation and steering mechanisms, the items can be estimated statistically with sufficient accuracy and thus

eliminates the need to resort to an analytical method [App. A]. A detailed weight breakdown is provided in Table 8.6; the values are presented in terms of percent total landing gear weight.

Table 8.6 Landing gear weight breakdown [2]

Component	Main assembly	Nose assembly
Rolling stock	**32.0**	**2.0**
Wheels	6.0	1.0
Tires	10.0	1.0
Brakes	16.0	0.0
Miscellaneous	0.0	0.0
Structure	**50.0**	**7.0**
Shock strut	32.0	4.0
Braces	12.0	1.0
Fittings	5.0	1.0
Miscellaneous	1.0	1.0
Controls	**7.0**	**2.0**
Total	**89.0**	**11.0**

Using the combined analytical and statistical approach presented here, the landing gear group weight for the Boeing Models 707, 727, 737, and 747 were calculated and compared with actual values. As presented in Table 8.7a, the analysis tends to underestimate the group weight as the aircraft takeoff weight increases. Linear regression analysis was used to calibrate the estimated group weights (W_{est}) so they agree with the actual values. Correction factors were calculated using the expression

$$f_c = 0.005W - 525 \tag{8.31}$$

where W is the aircraft weight. The correction factor is then combined with W_{est} to arrive at the calibrated landing gear group weight (W_{cal}), that is,

$$W_{cal} = W_{est} + f_c \tag{8.32}$$

The objective of this effort is to ensure that the discrepancy between the actual and estimated values will remain within a tolerable range. This is important when the analysis is used to examine the weight of landing gear for aircraft that are outside the existing pavement thickness database. The calibrated results are shown in Table 8.7b.

Table 8.7 Landing gear group weight comparison

a) Estimated group weight

Aircraft	Estimated, lb	Actual, lb	Est/Act
B737	4479	4382	1.02
B727	5976	6133	0.97
B707	9510	11216	0.85
B747	27973	31108	0.90

b) Calibrated group weight

Aircraft	Calibrated, lb	Actual, lb	Cal/Act
B737	4499	4382	1.03
B727	6301	6133	1.03
B707	10545	11216	0.94
B747	31138	31108	1.00